

## First Results of the TOTEM Roman Pots

---

**Jan Kašpar**<sup>\*†</sup>

*Institute of Physics of the AS CR Prague*

*E-mail: [jan.kaspar@cern.ch](mailto:jan.kaspar@cern.ch)*

The TOTEM experiment is dedicated to forward physics at the LHC accelerator at CERN. As one of its sub-detectors it includes a system of so-called Roman Pots, the purpose of which is the detection of very forward protons scattered from the IP5. In order to maximize the coverage for these very forward protons, the Roman Pots are movable beam-pipe insertions (to insert the detectors as close to the beam as safe) equipped with “edgeless” silicon sensors. This paper presents a collection of recent results related to the TOTEM Roman Pots and their sensors. In the first part we summarise the results that characterize the sensors – the efficiency at the active edge, the signal-to-noise ratio, the charge-sharing ratio, the average cluster-size and the reconstruction bias. All the collected results show that the sensors are fully efficient in  $\approx 50 \mu\text{m}$  from the physical edge. As an example of the results obtained during the commissioning of the Roman Pots, we mention the alignment based on recorded tracks. It is found to agree well with the optical alignment performed during the Roman Pot assembly. At the end, we show some of the first results obtained with LHC beams of energies 450 GeV and 3.5 TeV.

*19th International Workshop on Vertex Detectors*

*June 6 -11 2010*

*Loch Lomond, Scotland, UK*

---

<sup>\*</sup>Speaker.

<sup>†</sup>On behalf of the TOTEM collaboration.

## 1. Overview of TOTEM Experiment

The TOTEM experiment [1, 2] is an LHC experiment dedicated to forward hadronic phenomena. The three pillars of its physics programme are: an accurate measurement of the total pp cross section, a measurement of elastic scattering in a wide kinematic range and studies of diffractive processes. All these processes are characterized by the presence of forward particles in the final state. This feature brings special requirements for the detector apparatus. In particular, large pseudorapidity coverage – to detect most fragments from inelastic collisions and appropriate acceptance for outgoing diffractive and elastic protons. To accomplish these tasks, TOTEM comprises three sub-detectors: the telescopes T1 and T2 to detect inelastic collision products and a system of Roman Pots (RP) for forward proton detection. In this paper we will focus on the Roman Pot system, more information on the telescopes can be found in [1, 2].

The Roman Pots are placed symmetrically around the interaction point 5 (IP5). There are two stations at 147 and 220 m at each side of the IP (see Fig. 1). The elements of a station are shown in Fig. 2 – each station has 2 units, each unit is composed of top, horizontal and bottom pot, each pot contains a package of 10 hybrids and each hybrid hosts a strip silicon sensor. The sensors have strips oriented at  $45^\circ$  wrt. the edge facing the beam and are grouped in 5 back-to-back mounted pairs in the detector package (see Fig. 2 bottom middle). The thin window (Fig. 2 top middle) separates the sensors from the primary LHC vacuum. Its low material budget (as quantified in the picture) is extremely important to keep the interaction rate at a bearable level. The overlap between top, horizontal and bottom pots (Fig. 2 bottom right) is crucial for the alignment.

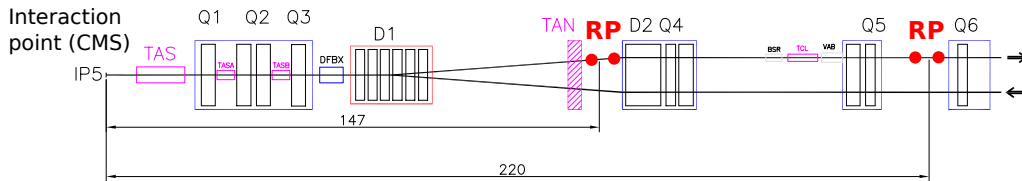


**Figure 1:** The scheme of the Roman Pot system (only the part on the right side of IP5 is shown). The black lines represent the beam-pipes of incoming and outgoing beams (see the arrows on the r.h.s.). The two RP stations are marked in red, each unit is drawn as a red dot.

In order to maximize the acceptance for forward protons, the detectors need to be as close to the beam as possible – this has two consequences. First, the RPs must be movable. They would be retracted to a safe position when beams are instable and would move close to the beam for data-taking. The second consequence, one has to minimize the gap between the outer edge of a RP (that is of the thin window) and the sensitive area of the sensors. This gap comprises three contributions – the thickness of the thin window, the space between the window and the sensors and the insensitive edge of the sensors. Standard planar silicon detectors have insensitive edges which are unacceptably large and therefore TOTEM has developed an “edgeless” type of silicon sensors.

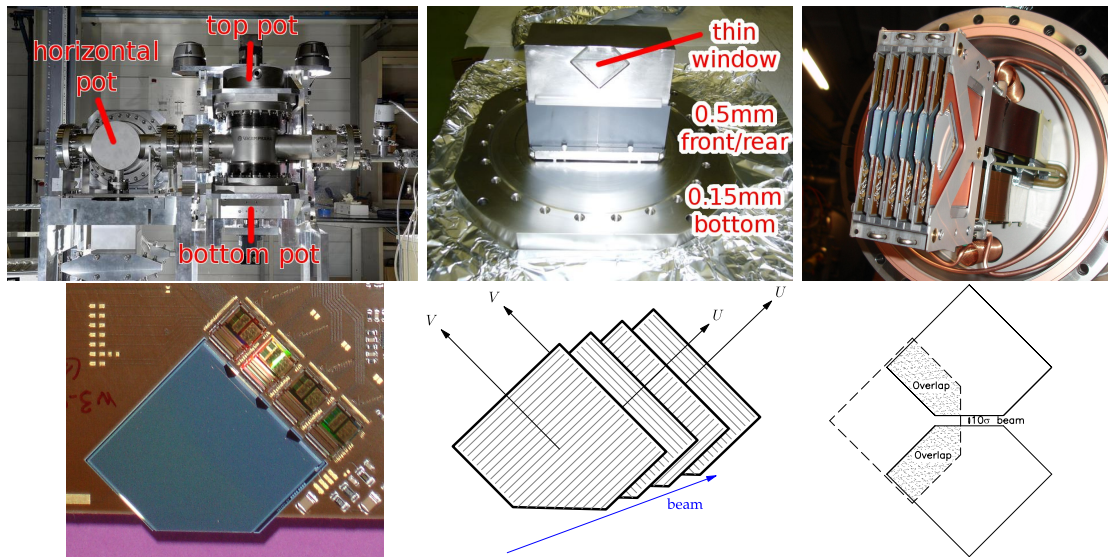


**Figure 2:** The elements of the Roman Pot system.

*Top row.* Left: a unit with top, horizontal and bottom pot. Middle: a pot with the thin window. Right: a package of 10 hybrids.

*Bottom row.* Left: a silicon sensor mounted on a hybrid with four read-out chips. Middle: the first 4 sensors in a package (the rest follows in the same way) with their strip orientations and the definition of U and V read-out directions. Right: the overlap of sensors in top, horizontal and bottom pots, in the view along the beam-line.

## 2. Edgeless Silicon Detectors with Current Terminating Structure

Silicon detectors fabricated with standard planar technology require terminating structures to reduce electric field maxima at the detector periphery to prevent the surface irregularities on the die cut from affecting the device performance, and to reduce the breakdown probability. These generally take the form of a sequence of floating guard rings surrounding the sensitive part of the device and adding an external dead volume.

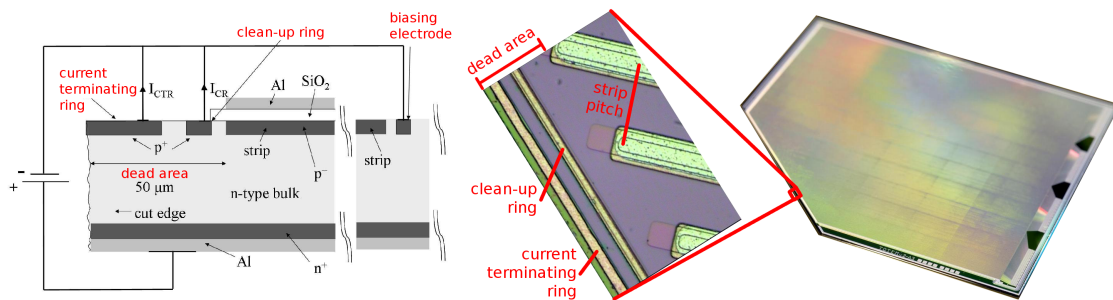


**Figure 3:** Scheme of edgeless silicon detectors with CTS. Left: diagram of the cross-section of a sensor and its biasing scheme. Right: a sensor with a microscope photograph of the edge area.

This ring structure, called “voltage-terminating structure”, controls the potential distribution between the detector’s sensitive area and the cut edge, thereby enabling the potential drop to vanish at the chip cut. The insensitive margin increases with the number of rings, and for high-voltage applications, as is the case for silicon detectors used in harsh radiation environments, it can be

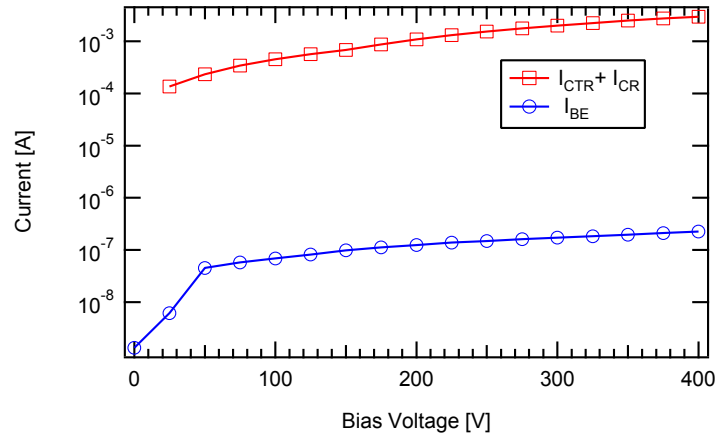


**Figure 4:** Current vs. voltage characteristics through the biasing electrode ( $I_{BE}$ ) and across a detector edge ( $I_{CTR} + I_{CR}$ ), measured at room temperature.

more than 1 mm wide. For the TOTEM experiment, the reduction of this dead space is vital. These requirements triggered the development of a new terminating structure that allows detectors fabricated with standard planar technology to reach full sensitivity within less than 100  $\mu\text{m}$  from the cut edge and to operate with high bias at room temperature.

For segmented devices with this new so-called Current Terminating Structure (CTS), the potential applied to bias the device must be applied also across the cut edges via a guardring running along the die cut and surrounding the whole sample. This external guard ring, also called “Current Terminating Ring” (CTR), which is separated from the biasing electrode (BE), collects the current generated in the highly damaged region at the cut edge, thereby preventing its diffusion into the sensitive volume. In this manner the sensitive volume can start at less than 50  $\mu\text{m}$  from the cut edge. To prevent any further diffusion of this edge current into the sensitive volume, another implanted ring, the Clean-up Ring (CR), can be placed between the CTR and the sensitive volume. The CTS and its biasing scheme are shown in Fig. 3.

In Fig.4, the I–V plot shows the low current flowing into the biasing electrode and confirms that virtually all the leakage current generated at the edge surface is collected by the CTR and the CR and will therefore not reach the sensitive bulk. This current, which can reach at room temperature few milliamperes at 200 V, does not affect at all the detector’s performance. This confirms the validity of the current termination approach and demonstrates that the leakage current in the sensitive bulk ( $I_{BE}$ ) is completely decoupled from the edge current ( $I_{CTR} + I_{CR}$ ).

More details on the CTS conception can be found in [3, 4].

The sensors are single-sided AC coupled  $p^+ - n$  microstrip detectors with 512 strips and a pitch of 66  $\mu\text{m}$  processed on very high resistivity n-type silicon wafers ( $> 10 \text{ k}\Omega\text{cm}$ ) that are 300  $\mu\text{m}$  thick. All of them have the CTS on the edge facing the beam. At one end of the strips, an integrated pitch adapter reduces the inter-strip distance from 66 to 44  $\mu\text{m}$  thereby producing four separated groups of 128 channels that are directly bonded to VFAT read-out chips.

The prototypes were extensively tested with muon beam in the extraction point X5 at the SPS accelerator. The full report can be found in [5], here we will pick up the most relevant results only. The test setup included four detector packages, two of them were used as reference detectors

defining a track, the other two were actually tested. The uncertainty of the track interpolation in the test detectors was below  $10 \mu\text{m}$ . APV25 was used as the read-out chip – as this is an analogue chip, signal amplitude was available too.

In Fig. 5, you can find efficiency curves for two tested sensors. The  $w$  coordinate is perpendicular to the cut edge and is increasing with the distance from the edge. All detectors tested reach the full efficiency in within  $60 \mu\text{m}$  from the physical edge (marked by the red line). The full efficiency is of about 95% only because of unbonded and noisy strips.

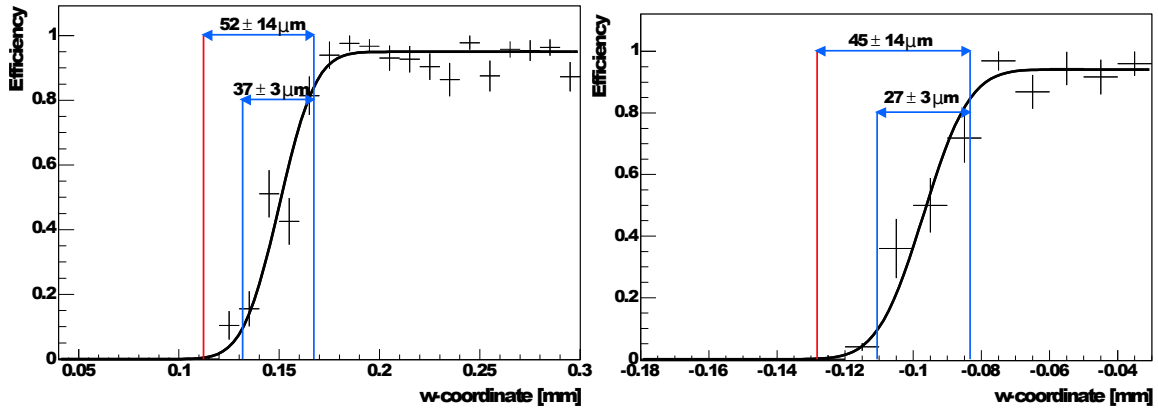


**Figure 5:** Efficiency of two sample sensors as a function of the distance to the edge ( $w$ ). The position of the cut edge is marked by the red line. The blue lines show 10% to 90% efficiency rise intervals.

Fig. 6 shows signal-to-noise plots. The most probable  $S/N$  value of 27 guarantees an excellent noise/signal separation. On the right side of the figure, you can see  $S/N$  dropping as approaching the physical edge.

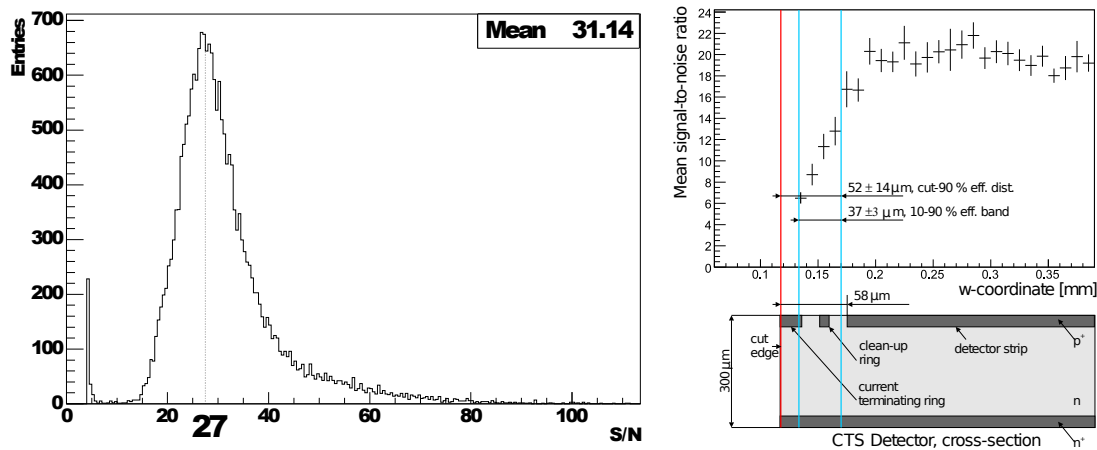


**Figure 6:** Signal-to-noise ratio. Left: histogram with the noise peak cut off at  $S/N = 3$ . Right:  $S/N$  as a function of the edge distance. The physical edge is represented by the red line, the blue band corresponds to 10 to 90% efficiency rise.

The left plot of Fig. 7 shows a profile of charge sharing ratio

$$\rho = \frac{Q_{\text{main strip}}}{Q_{\text{cluster}}},$$

where  $Q_{\text{main strip}}$  is the charge collected by the main strip of a cluster and  $Q_{\text{cluster}}$  is the charge from the entire cluster. As expected for a well-behaving sensor,  $\rho$  is close to 1 for hits near strip centers and reduces for hits in between strips. It is important that it remains true also near the cut edge (see the upper part of Fig. 7 left). The red color in that area indicates that most of the charge is collected by one strip and thus the resolution does not deteriorate even very close to the cut edge. A similar trend can be observed in the plot of average cluster size (Fig. 7 right) – hits at the edge form mostly 1-strip clusters. In both plots of Fig. 7 one can clearly see a change of shape near the strip's end. This is caused by an alternation in the charge-collection direction. In the inner part of the sensor the direction is perpendicular to the strips, but near the edge it becomes perpendicular to the edge. This effect introduces a reconstruction bias which is quantified in Fig. 8 left. But since this effect is understood, data can be fully corrected for it during software processing.

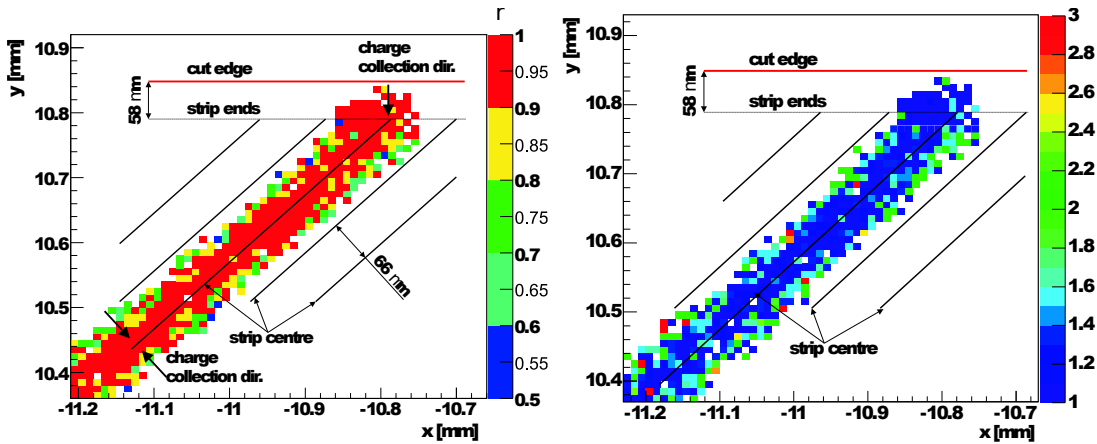


**Figure 7:** Left: charge sharing ratio  $\rho$ . Right: average cluster size. Both: physical edge drawn in red, strip centers in black. To increase statistics (and thus reduce fluctuations), the data from all strips have been overlapped.

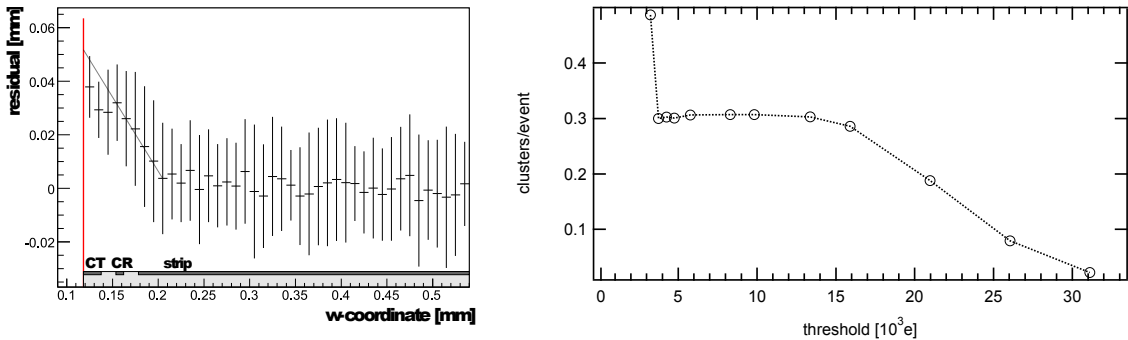


**Figure 8:** Left: profile of residuals near the cut edge (drawn in red). A non-zero mean value represents a reconstruction bias. Right: results of a threshold scan with a pion beam.

For the final electronics, the VFAT2 chip was chosen instead of APV25 as the read-out chip. As VFAT2 is a digital chip, the signal-to-noise ratio can be obtained by the terms of a threshold scan – see Fig. 8 right. The plateau starts at about 3000 e, this corresponds to the end of the noise peak. The plateau extends to about 15000 e, this is where the signal peak starts. The efficiency drops to half around 22000 e, which roughly corresponds to the maximum of the signal peak. Analyzing

the results for low thresholds (not visible in the plot), one can find the noise peak maximum around 1 000 e. Putting it all together, one may expect the signal-to-noise ratio in the range 20 to 25, which is compatible to the results obtained with APV25 (see Fig. 6 left).

### 3. Commissioning Tests

All RP detectors have been tested prior to their installation. The tests were done either with muon beam or with cosmic rays. The data recorded were used to benchmark our alignment software and to obtain first alignment corrections. These were compared to the results of an optical alignment performed during the assembly of the detector packages, as it is shown in Fig. 9. The optical alignment consists of using a microscope to measure the positions of the fiducial marks engraved on the silicon sensors. The alignment based on real data performs an analysis of track residuals, that is the differences between measured hits and track fits. In this analysis, sensors' shifts and rotations around the beam direction are optimized. For a brief review of TOTEM's alignment strategy see [6].

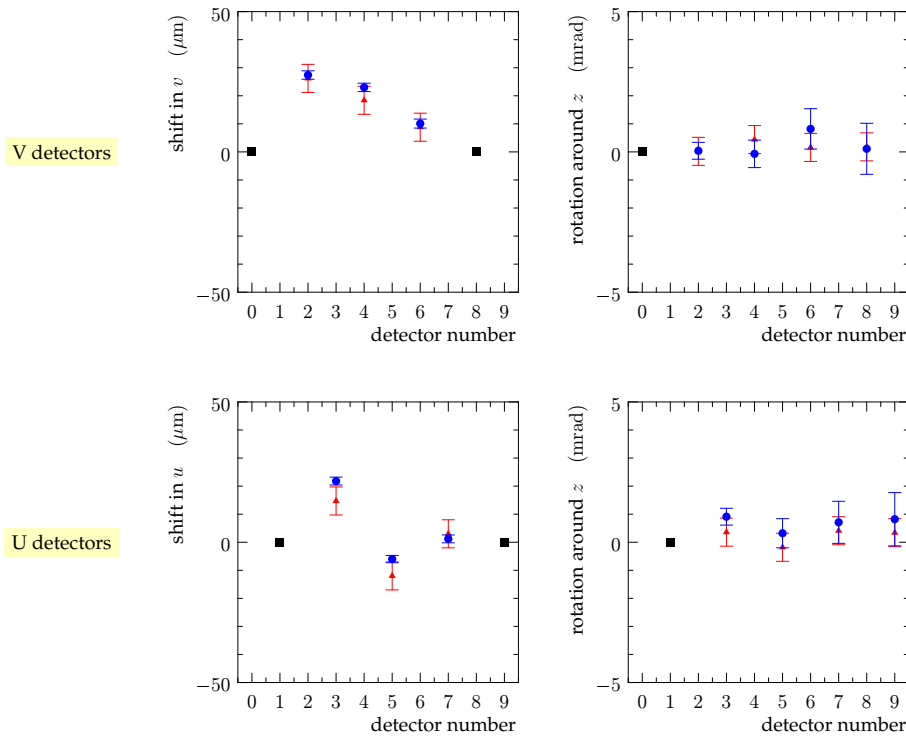


**Figure 9:** Comparison of the track-based (blue triangles) and the optical (red dots) alignment. The U and V directions are defined in Fig. 2 bottom middle, the  $z$  axis coincides with the beam. The track-based alignment cannot resolve all alignment parameters – some misalignment modes are inaccessible to it. To overcome this problem, one has to apply constraints that fix these inaccessible modes. Here, we have fixed the positions of detectors 0, 1, 8 and 9 and the rotations of detectors 0 and 1 (these constraints are marked by black squares). The same constraints have been applied to the optical alignment. For the fixed parameters, the alignment corrections are zero by definition.

#### 4. First LHC data

The very first data-taking with a RP moved into the LHC beam-pipe took place in December 2009. At that time a beam of the injection energy of 450 GeV was used. Only one pot was allowed to move in, its edge reached the distance of  $4.5\sigma$  from the beam. A compilation of results from this test is shown in Fig. 10. The peaks in the U (detector 2) and V (detector 1) hit profiles can be traced (dashed blue line) to the point on the detector that is the closest to the beam. The number of reconstructed tracks was low because of two reasons. First, a trigger on a bunch-crossing was used and thus most events were empty. Second, as the pot was very close to the beam, most non-empty events were of high occupancy and such events are very difficult to reconstruct.

In April 2010 we started to take data at 3.5 TeV beams, making use of the trigger capability of the RP system. An example event is shown in Fig. 11.

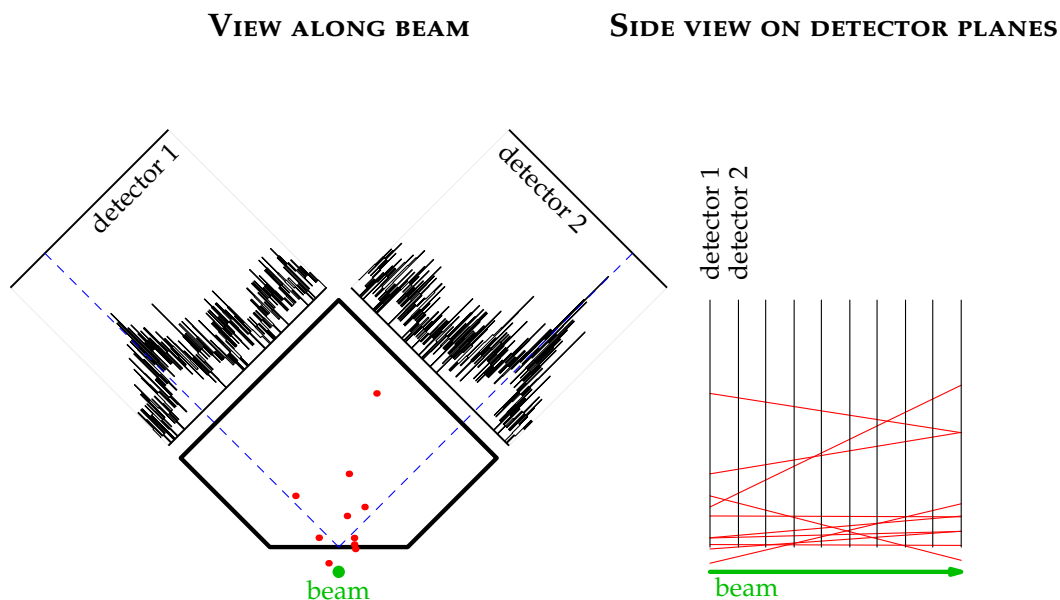


**Figure 10:** Some results from the first data-taking with RPs at the LHC. The reconstructed tracks are drawn in red – as lines in the side view, as dots in the front view. The dots show the track extrapolated to detector 1, that is why the one hit outside the detector area. The two histograms show hit profiles as measured by the first two detectors.

#### 5. Summary and Outlook

Both stations at 220 m are fully equipped and operational with more than 99% of channels working. More detector packages will be installed to the 147 m stations during the next technical stop of the LHC.

At the time of writing of this paper, the RPs are taking data at  $20\sigma$  (verticals) and  $25\sigma$  (horizontal) from the beam and thus will soon start contributing to advances in understanding the forward hadronic physics.

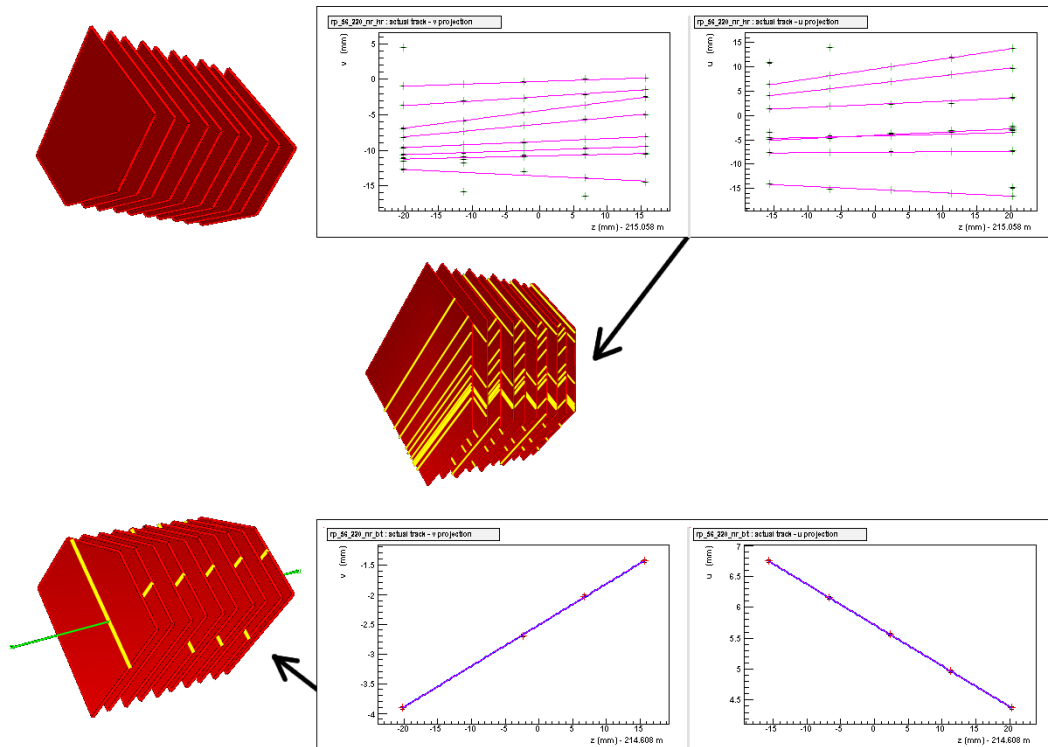


**Figure 11:** An event seen with RPs in the garage position. There is a clean track (drawn in green) in the bottom pot and a shower the horizontal one. The silicon sensors are drawn in red, the yellow lines represent strips fired in the event. The boxes show the measured hits in V (left) and U (right) projections. Track candidates are drawn in violet. There is no overall track fit for the horizontal pot (with shower) since it is not possible to match U and V track candidates in this case.

## References

- [1] TOTEM: Technical Design Report, CERN-LHCC-2004-002 (2004); addendum CERN-LHCC-2004-020.
- [2] G. Anelli *et al.* [TOTEM Collaboration], JINST **3**, S08007 (2008).
- [3] G. Ruggiero *et al.* [TOTEM Collaboration], IEEE Trans. Nucl. Sci. **52** (2005) 1899.
- [4] G. Ruggiero *et al.* [TOTEM Collaboration], Nucl. Instrum. Meth. **A 604** (2009) 242–245.
- [5] H. Niewiadomski *et al.* [TOTEM Collaboration], “Reconstruction Performance of Silicon Detectors with Reduced Edge Insensitive Volume Manufactured in CTS and 3D-Planar Technologies”, to be published.
- [6] J. Kašpar [TOTEM Collaboration], 13<sup>th</sup> International Conference on Elastic and Diffractive Scattering, CERN (2009).